Supporting Information for

Ring Fusion Attenuates the Device Performance: Star-Shaped Long Helical Perylene Diimide Based Non-Fullerene Acceptors

Mingliang Wu,[a,b#] Jian-Peng Yi,[b#] Juan Hu,[a] Ping Xia,[b] Huan Wang,[a] Fei Chen,[a] Di Wu,[b*] Jianlong Xia[a,b*]

[a]State Key Laboratory of Advanced Technology for Materials Synthesis and Processing, Center of Smart Materials and Devices, Wuhan University of Technology No. 122 Luoshi Road, Wuhan 430070, China

[b]School of Chemistry, Chemical Engineering and Life Science, Wuhan University of Technology No. 122 Luoshi Road, Wuhan 430070, China

[#]These authors contributed equally to this work.

Email: D.W.(chemdwu@whut.edu.cn); J. X. (jlxia@whut.edu.cn)

Table of the contents

1. General Information

All chemical reactions were conducted in oven-dried or flame-dried glassware. A homo-built flow photochemical reactor[1] was used to synthesize the TPDI3 and FTPDI3 with Au Light CEL-LB70 as the light source. All the chemicals and starting materials were purchased from commercial sources without further treatment unless specially noted. The commercially available polymer donor PTB7-Th was purchased from Solarmer Materials Int. with a MW over 40000 and a PDI of 1.8-2.0. Compounds perylene diimide,[2] monobromoperylene diimide[3] and perylene diimide dimer[4] were synthesized according to literature procedures.

^{1}H NMR and ^{13}C NMR spectra were measured on Bruker DRX 500 or Varian Mercury plus-400. MALDI-TOF Mass spectrum was measured with AB Sciex 5800. UV-Vis spectrum was recorded on Shimadzu UV-1800. Cyclic voltammograms (CVs) were obtained on CHI660E electrochemical workstation. A three-electrode one-compartment cell containing a solution of the analyte and supporting electrolyte (tetrabutylammonium, ($[NBu_4]PF_6$), 0.1M) in dry CH_2Cl_2 was utilized. A 500 μm diameter platinum-disk as working electrode, a platinum-wire as counter electrode, and an Ag/AgCl as reference electrode at a scanning rate of 100 mV/s. The atomic force microscope (AFM) images were recorded by a Dimension Icon AFM (Bruker). Transmission electron microscope (TEM) images were performed on a JEOL 2010 TEM at an accelerating voltage of 100 kV. XRD data were performed by D/MAX-RB, which equipped with a linear Scintillation detector and under the specular measurement type, all these sample were spin coated on quartz glass substrates.

Thermogravimetric analysis (TGA) was carried out on a tainstruments SDT Q-600 under a nitrogen atmosphere at a heating rate of 10 ^{o}C/min.

In order to reduce the computational costs, it is reasonable to replace the long C_6H_{11} side chain attached to each imide N with a single H atom. The geometry optimizations of **TPDI3** and **FTPDI3** were performed using the density functional theory (DFT) combining with the Perdew, Burke and Ernzerhof (PBE) functional[5-6] and the Pople's 6-31G(d) basis set. Choosing this level is a result of the compromise between the computational accuracy and the costs, because of the large size of these two molecules, of which consist of around 350 atoms. Frequency analysis were then performed to confirm the geometry stability without imaginary frequency. All calculations were carried on the Gaussian16 quantum chemistry package.[7] The HOMOs and LUMOs of these two molecules were obtained by using the Multiwfn program[8] and visualized *via* the VMD package.[9]

Device fabrication: The inverted devices were fabricated with the structure of ITO/ZnO/active

layer/MoO_3/Ag. The pre-patterned (sheet resistance, 15 Ω/sq) ITO-glass substrates were sequentially cleaned in ultrasonic bath with detergent (Alconox Inc.), de-ionized water, acetone and isopropanol. The oven-dried substrates were then treated by an oxygen plasma (180 W) for 5 min. The ZnO precursor solution (110 mg/mL) was prepared by dissolving 0.22 g $ZnAc_2 \cdot 2H_2O$ in 2 mL 2-methoxyethanol and 0.056 mL ethanol amine and then stirred for at least 24h before use. The solution was filtered with polyether sulfone (PES) filters. The ZnO precursor solution was spin-cast onto ITO substrate with spinning rate of 5000 rpm for 60s and the thickness was ~32 nm. The as-cast film was then annealed in ambient circumstance upon 150 ^oC for 60 min to form a compact ZnO layer. The blend solutions of PTB7-Th:TPDI3 and PTB7-Th:FTPDI3 (D/A ratio, 1:1, weight ratio) mixtures were all processed with o-dichlorobenzene (o-DCB) with an identical concentration of 20 mg mL^{-1}. All these solutions were heated at 60 ^oC and stirred overnight (or 100 ^oC for 3h) to obtain well-mixed blend solutions. The active layer thicknesses of these three devices were carefully optimized through spinning rate variation (1200, 1500, 1800, 2000 and 2500 rpm). And, the spinning duration was fixed at 50s. The active layers were thermal annealed at 80 ^oC in glove box for 10 min to get rid of residual solvent. A MoO_3 (8 nm) layer and an Ag layer (100 nm) electrode were sequentially deposited by thermal evaporation using a shadow mask under a vacuum of $<1.0\times10^{-4}$ pa. The effective device area, defined by the overlap region of ITO and Ag electrodes, was 0.0625 cm^2.

The *J-V* measurements were conducted under AM 1.5G illumination at 100 mW cm^{-2} using an AAA solar simulator (SP94023A-SR1, NEWPORT). The illumination intensity was calculated with a standard photovoltaic cell (91150V) which incorporated with a quartz window (1000P072). External quantum efficiency (EQE) was determined by an EQE system (Zolix, China). The film thicknesses were determined on Bruker DektakXT Stylus Profling System.

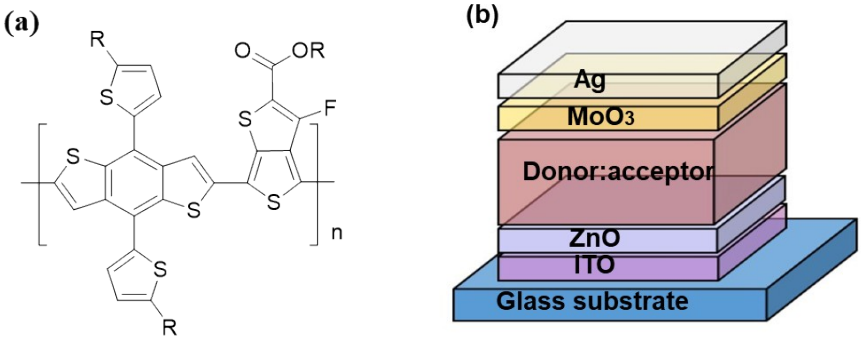

Fig. S1 (a) chemical structure of PTB7-Th (electron donor) and (b) structure of OSCs.

2. Material Synthesis

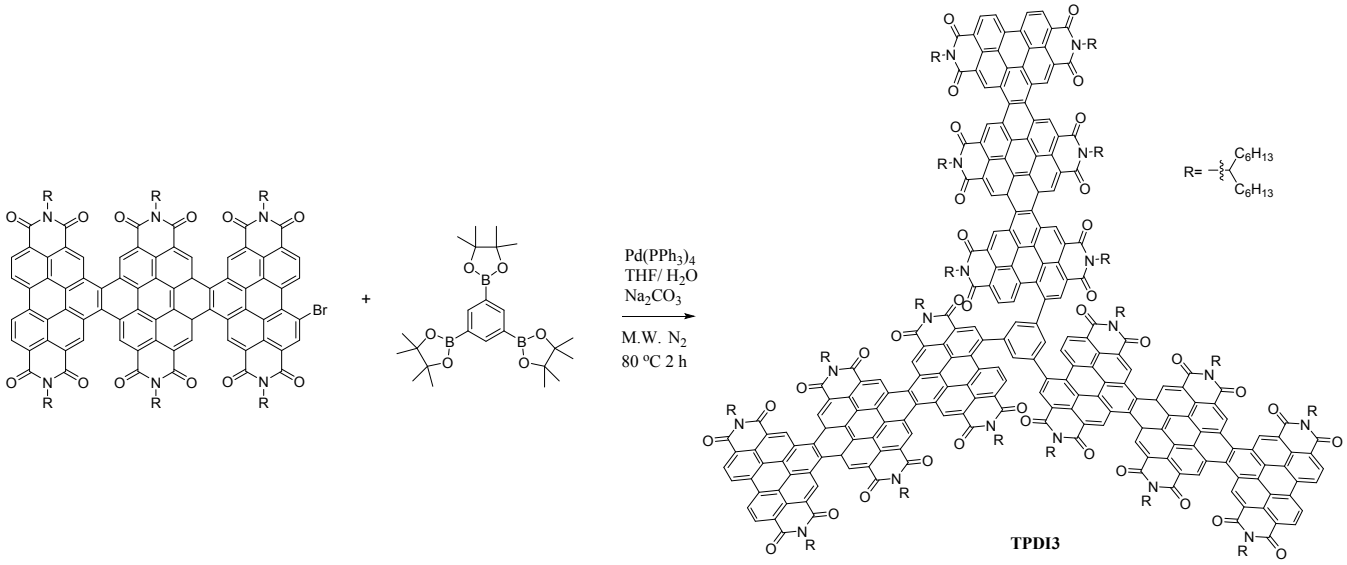

Scheme S1 Synthetic route of TPDI3

To a mixture of monobromo-PDI3 (PDI3-Br, 400 mg, 0.168 mmol), 1,3,5-Benzenetriboronic acid tris(pinacol) ester (**1**, 21.2 mg, 0.046 mmol), Na_2CO_3 (1 g), and Tetrakis(triphenylphosphine)palladium(0) (30 mg, 0.026 mmol) in microwave tube, degassed THF/H_2O (4:1, 20 ml) was added. The reaction was performend by microwave reactor at 80 °C for 2 hours. After cool down to room temperature, the mixture was extract with DCM and washed with water. Them the solution was dried over Na_2SO_4 and concentrated under reduced pressure. The crude solid was purified by silica gel chromatography (eluted with petroleum ether/CH_2Cl_2 from 1:1 to 1:3), further recrystallization with CH_2Cl_2/methanol afforded the target molecule **TPDI3** as dark red laminar solid (159 mg, 49 %). ^{1}H NMR (500 MHz,) δ 10.91 (s, 11H), 10.58 (s, 11H), 10.21 (s, 2H), 9.79 (s, 1H), 9.51 (s, 8H), 9.12 (d, J = 84.3 Hz, 12H), 8.66 (s, 3H), 5.40 (s, 6H), 5.27 (s, 12H), 2.29 (s, 36H), 1.97 (s, 36H), 1.21 (s, 288H), 0.77 (s, 108H). ^{13}C NMR (101 MHz, CDCl3) δ 165.34, 165.19, 164.97, 164.87, 164.20, 163.84, 163.63, 134.10, 127.46, 127.31, 126.97, 126.30, 125.95, 124.97, 124.43, 123.97, 122.18, 55.56, 55.46, 55.19, 55.02, 32.67, 32.48, 31.82, 31.73, 29.71, 29.33, 27.22, 27.12, 26.96, 22.65, 22.52, 14.09, 13.93. HRMS (MALDI-TOF): $[TPDI3+Na]^+$ calculated for 7016.11; found 7016.89.

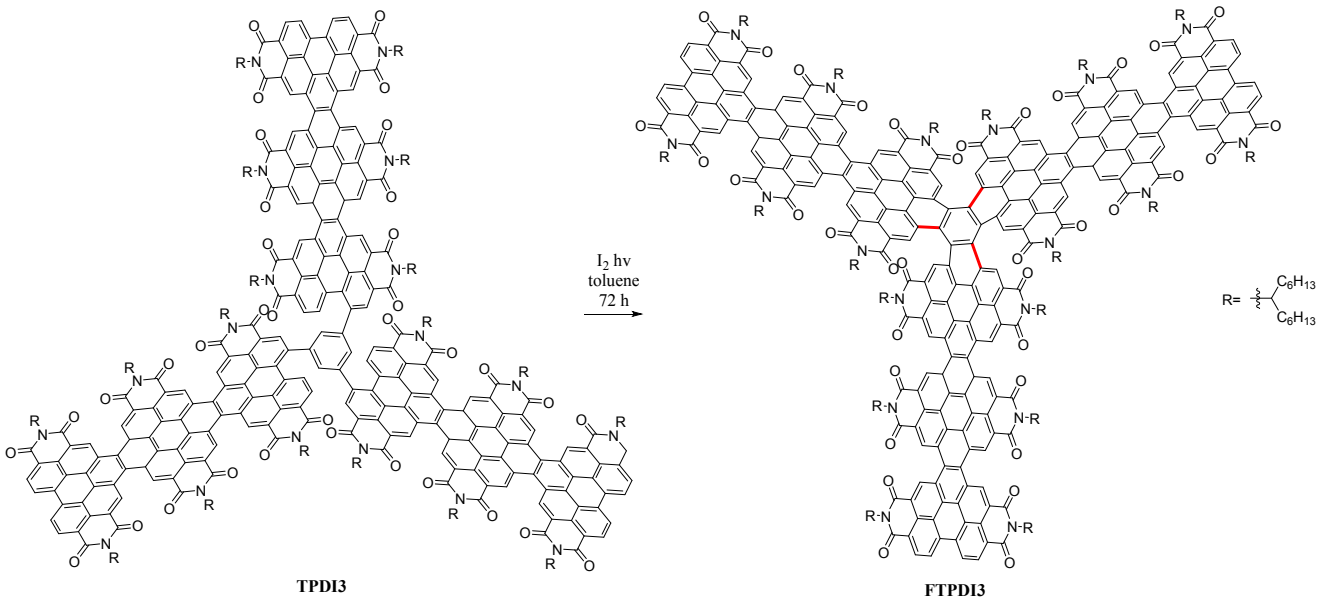

Scheme S2 Synthetic route of FTPDI3

TPDI3 (370 mg, 0.529 mmol) was dissolved in 400 ml toluene in a 500 ml round bottom flask, and 200 mg of I_2 was added. The reaction mixture solution was drawn into a home-built flow reactor. The reaction mixture was repeatedly pumped through the flow reactor with a retention time of 72 hours. The solvent was removed using vacuum rotary evaporator and the crude residue was washed with methanol to remove excessive iodine. The crude red solid was then purified with silica gel column using petroleum ether/CH_2Cl_2 as eluent. And the final product of FTPDI3 was obtained as a red solid (150 mg, 40%). ^{1}H NMR (500 MHz, Chloroform-d) δ 11.39 (s, 8H), 11.04 (s, 10H), 10.77 (s, 8H), 10.46 (s, 3H), 9.60 (s, 6H), 9.31 (s, 7H), 5.53 (d, J = 94.3 Hz, 18H), 2.54 (d, J = 71.6 Hz, 36H), 2.11 (d, J = 74.5 Hz, 36H), 1.31 (s, 288H), 0.87 (s, 108H). ^{13}C NMR (126 MHz, CDCl3) δ 165.05, 164.39, 134.14, 127.42, 127.06, 125.99, 125.11, 124.73, 124.48, 123.99, 122.42, 55.64, 55.25, 32.68, 31.90, 31.85, 29.42, 29.36, 27.29, 27.15, 22.70, 22.67, 14.11, 14.08. HRMS (MALDI-TOF): $[FTPDI3+Na]^+$ calculated for 7010.07; found 7010.38.

3. Thermal Gravimetric Analysis (TGA)

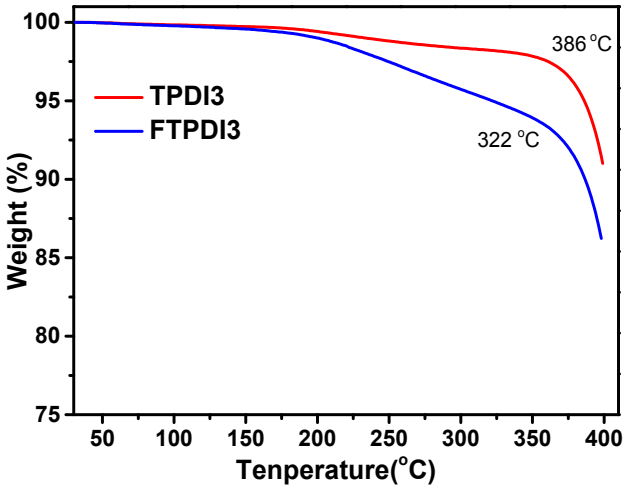

Fig. S2 Thermogravimetric analysis (TGA) result of TPDI3 (red line) and FTPDI3 (blue line) with a heating rate of 10 °C/min under nitrogen.

4. DFT Calculation

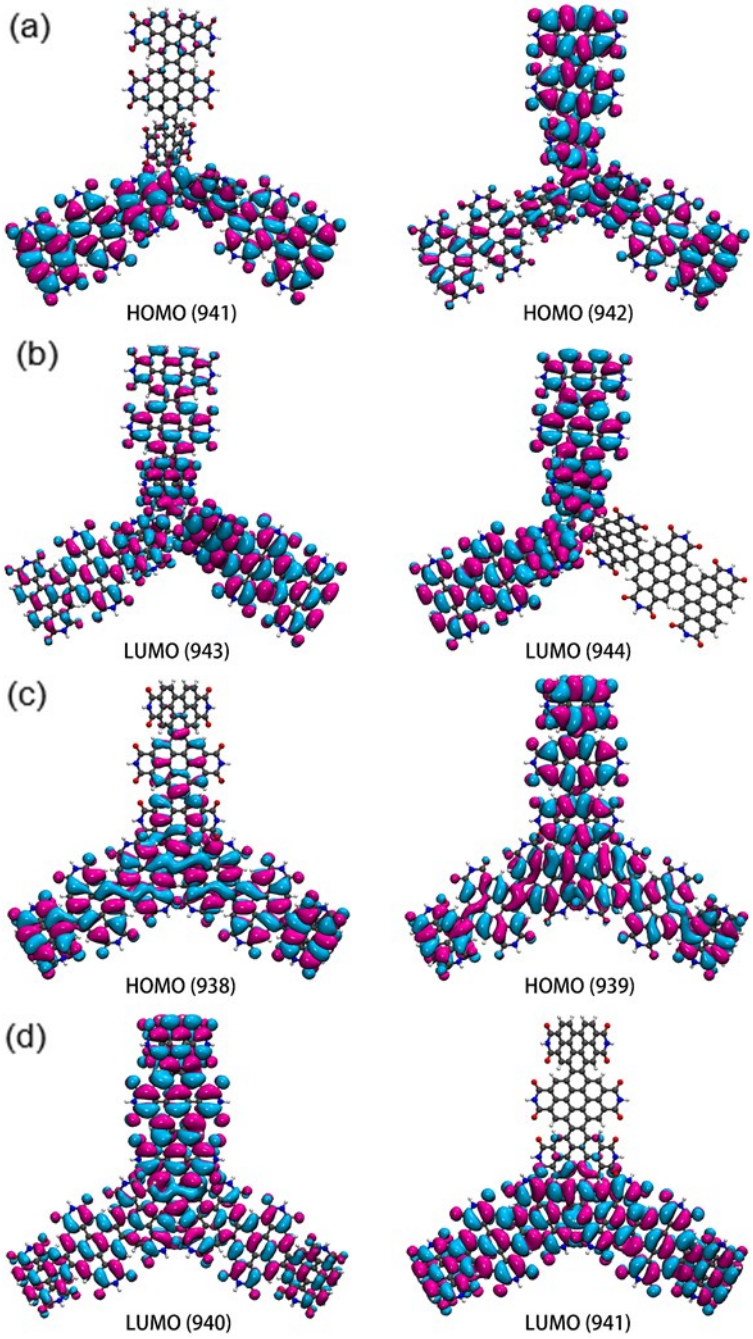

Fig. S3 HOMOs and LUMOs of **TPDI3** (a and b) and **FTPDI3** (c and d). Orbitals displayed at an isovalue of 0.005

Table S1. The HOMO, LUMO Energies and their Energy Gap of **TPDI3** and **FTPDI3**.

Species	E(HOMO) / eV	E(LUMO) / eV	E_{gap} / eV
TPDI3	−5.738	−4.366	1.372
FTPDI3	−5.732	−4.317	1.416

5. UV-Vis in Solution and Cyclic Voltammograms (CVs)

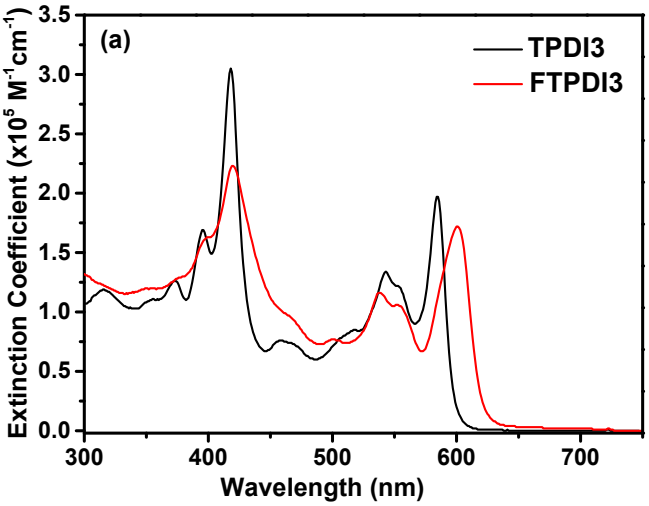

Fig. S4 UV-Vis absorption spectra for (a) TPDI3 and FTPDI3 in the $CHCl_3$ solutions of a concentration of 1.0×10^{-6} M.

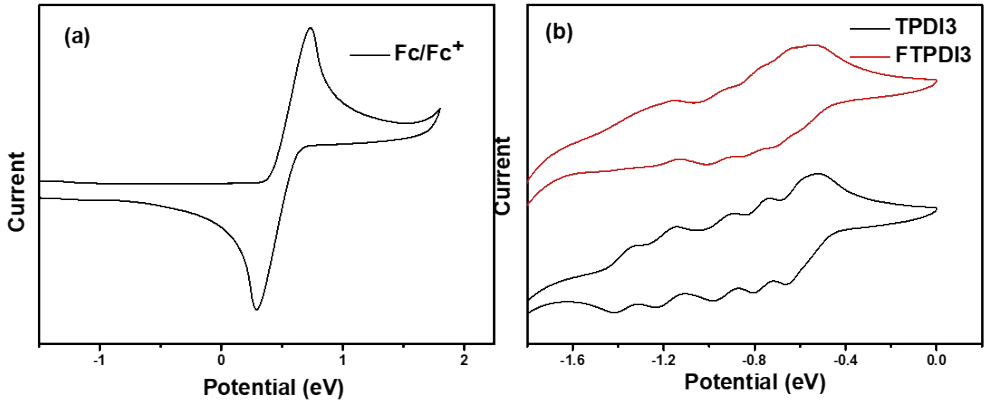

Fig. S5 Cyclic voltammograms (CVs) for （a） Fc/Fc$^+$, (b) TPDI3 and FTPDI3 at a scanning rate of 100 mV/s in dry DCM.

6. The photovoltaic performance of the devices

Table S2. The summary devices parameters of PTB7-Th:TPDI3 under different D/A mass ratio.

PTB7-Th:TPDI3 mass ratio	V_{oc} (V)	J_{sc} (mA/cm^2)	FF (%)	PCE (%)
1:0.5	0.763	16.40	61.6	7.72
1:0.8	0.767	16.03	64.7	7.95
1:1.0	0.767	16.49	65.1	8.24
1:1.3	0.763	15.92	63.7	7.73
1:1.5	0.771	14.85	66.6	7.63
1:2.0	0.772	14.82	66.2	7.58
1:2.5	0.770	13.99	63.6	6.86

Each averaged parameter was calculated from 16 individual devices.

Table S3. The photovoltaic performance parameters for the OSCs based on PTB7-Th:TPDI3.

PTB7-Th : TPDI3-8010	V_{oc} (V)	J_{sc} (mA/cm^2)	FF (%)	PCE (%)
DIO-0.25%	0.776	16.60	67.0	8.63
DIO-0.50%	0.774	16.32	67.3	8.51
DIO-0.75%	0.776	16.29	67.1	8.48
DIO-1.00%	0.773	16.92	66.1	8.64
DIO-1.50%	0.770	16.51	65.6	8.34
DIO-2.00%	0.771	16.12	65.2	8.10
DIO-2.50%	0.770	15.64	63.3	7.62
DIO-3.00%	0.77	14.08	66.2	7.19

Each averaged parameter was calculated from 16 individual devices.

Table S4. The photovoltaic performance parameters for the OSCs based on PTB7-Th:FTPDI3.

PTB7-Th : FTPDI3-8010	V_{oc} (V)	J_{sc} (mA/cm^2)	FF (%)	PCE(%)
DIO-0.5%	0.769	15.76	61.5	7.46
DIO-1.0%	0.773	15.16	62.8	7.36
DIO-1.5%	0.778	14.82	64.7	7.46
DIO-2.0%	0.774	14.2	63.7	6.99
DIO-2.5%	0.783	13.72	64.8	6.96
DIO-3.0%	0.78	12.94	62.6	6.32

Each averaged parameter was calculated from 16 individual devices.

Table S5. The summary devices parameters of different donors and PDI-oligomers acceptors.

Donor:Acceptor	V_{oc} (V)	J_{sc} (mA/cm^2)	FF (%)	PCE (%)	Ref.
PBDTT-TT:1	13.5±0.2	0.796±0.005	55±1	6.05	10
PTB7-Th:PDI3	14.5	0.81	67	0.79	
PTB7-Th:PDI3	15.2	0.80	68	8.3	11
PTB7-Th:2	15.1	0.8	62.9	7.6	12
PTB7-Th:SNTP	15.22±0.2 2	0.77±0.00	60±0.01	7.17	13
PTB7-Th:PFPDI-2T	14.47	0.73	65	6.39	14
PTB7-Th:PFPDI-Se	13.96	0.76	62	6.58	15
PTB7-Th:PFPDI-DTBT	14.13	0.76	58	6.23	16
PTB7-Th:NDP-V	17.07	0.74	67	8.59	17
PTB7-Th:(7,6)sSWCNTs:hPDI3	14.6	0.81	54.0	6.4	18
PTB7-Th:FPDI-Se	14.78	0.80	56.1	6.61	19
PTB7-Th:TPDI2	15.85	0.777	62.55	7.84	20
PTB7-Th:FTPDI2	16.77	0.790	61.67	8.28	
PTB7-Th:TPDI3	16.75	0.783	67.4	8.84	This work

PTB7-Th:FTPDI3	16.11	0.770	63.9	7.93

* Those data were obtained from the reference.

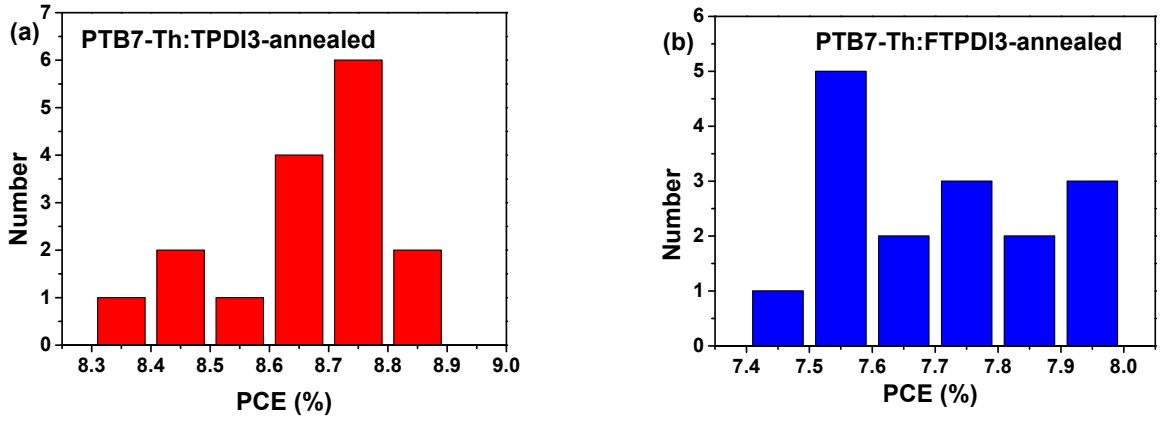

Fig. S6 The PCE distribution of the optimized devices based on (a) PTB7-Th:TPDI3 and (b) PTB7-Th:FTPDI3. Each content was obtained from 16 individual devices.

7. The integration of the EQE

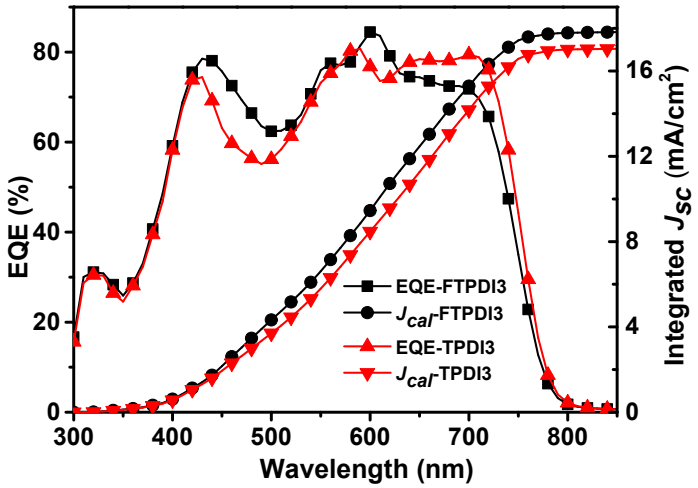

Fig. S7 The EQE of TPD3(red triangles), FTPDI3 (black squares) and the integration of EQE for TPDI3 (red inverted triangles) and FTPDI3 (black spheres).

8. Photoluminescence quenching experiment

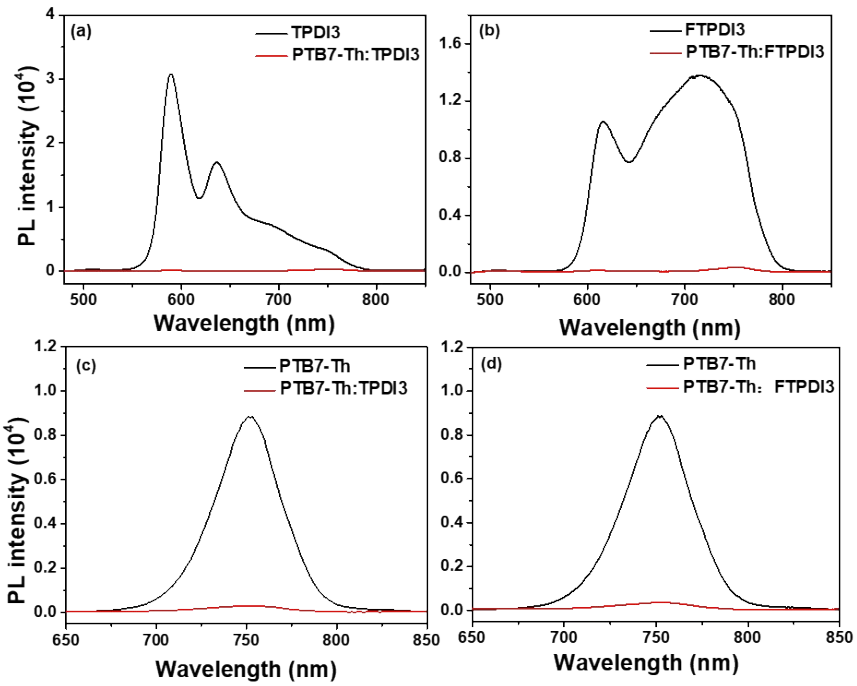

Fig. S8 The photoluminescence (PL) spectra (a) pure film of TPDI3 and blend films of PTB7-Th:TPDI3, (b) pure film of FTPDI3 and blend films of PTB7-Th:FTPDI3; (c) pure film of PTB7-Th and blend films of PTB7-Th:TPDI3, (h) pure film of PTB7-Th and blend films of PTB7-Th:FTPDI3. All those films were annealed upon 80 ^{o}C in glove box for 10 min.

Table S6. PL quenching efficiency of the neat film of donor (PTB7-Th), acceptor (TPDI3 and FTPDI3) and their blend films.

D/A	PL Quenching efficiency (%)	
	Quenching induced by electron transfer	Quenching induced by hole transfer
PTB7-Th:TPDI3	94.4	98.4
PTB7-Th:FTPDI3	93.0	97.7

9. The light density dependent J_{sc} and V_{oc} measurements

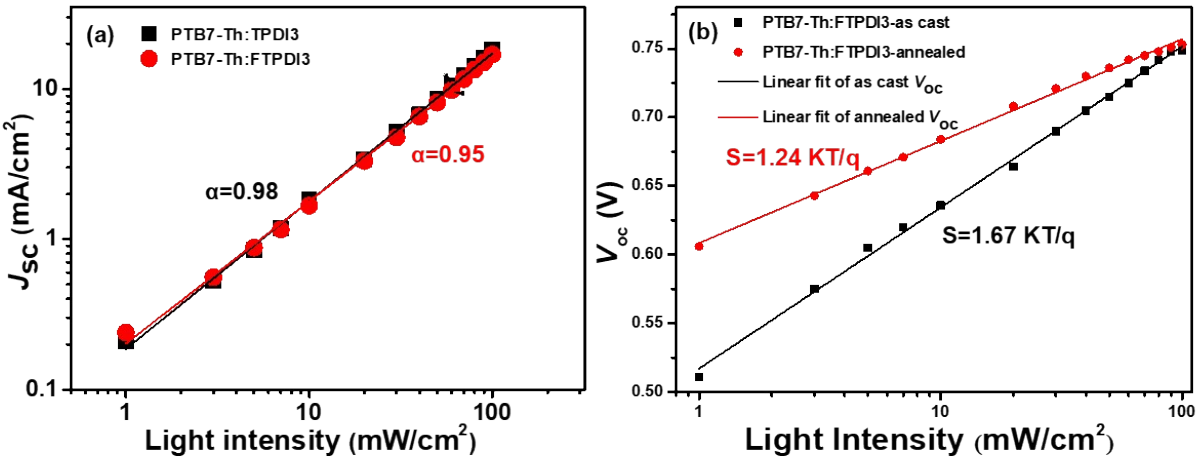

Fig. S9 (a) The dependence of J_{sc} on light density with the corresponding fitting results for the PTB7-Th:TPDI3 and PTB7-Th:FTPDI3-based devices; (b) the dependence of V_{oc} on light density with the corresponding fitting results for the as cast and annealed PTB7-Th:FTPDI3-based (annealed upon 80 ^{o}C for 10 min) devices.

10. Microscopic morphology characterizations

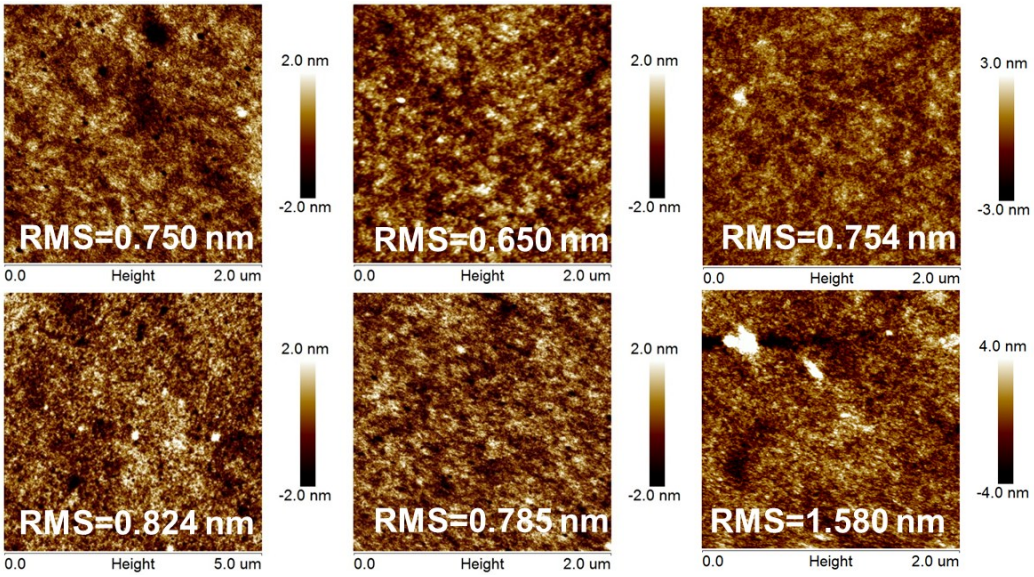

Fig. S10 The atomic force microscope (AFM) images of (a, b, c) PTB7-Th:TPDI3 and (d, e, f) PTB7-Th:FTPDI3. (a, d) were the as-cast films, (b, e) were the films annealed upon 80 ^{o}C for 10 min, and (c, f) were the annealed films with 1% DIO additives.

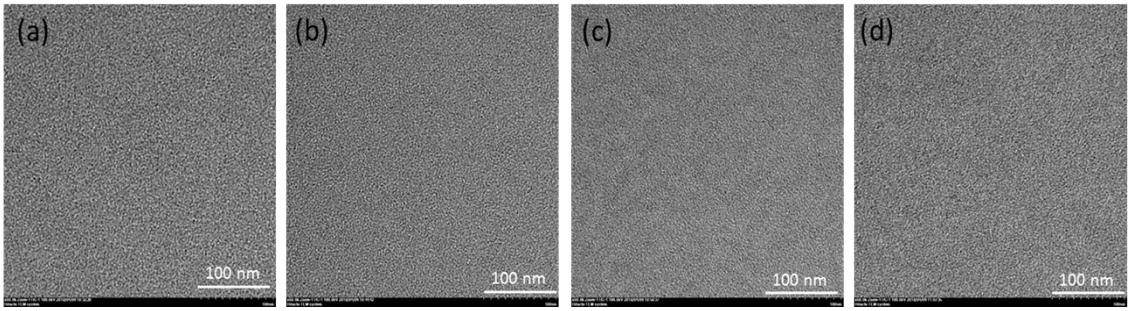

Fig. S11 The transmission electron microscope (TEM) images of (a) as-cast PTB7-Th:TPDI2 films, (b) annealed PTB7-Th:TPDI3 films, (c) as-cast PTB7-Th:FTPDI3 films and (d) annealed PTB7-Th:TPDI3 films. (The annealed films were undergoing thermal annealed at 80 ^{o}C for 10 min).

11. ^{1}H and ^{13}C NMR spectra

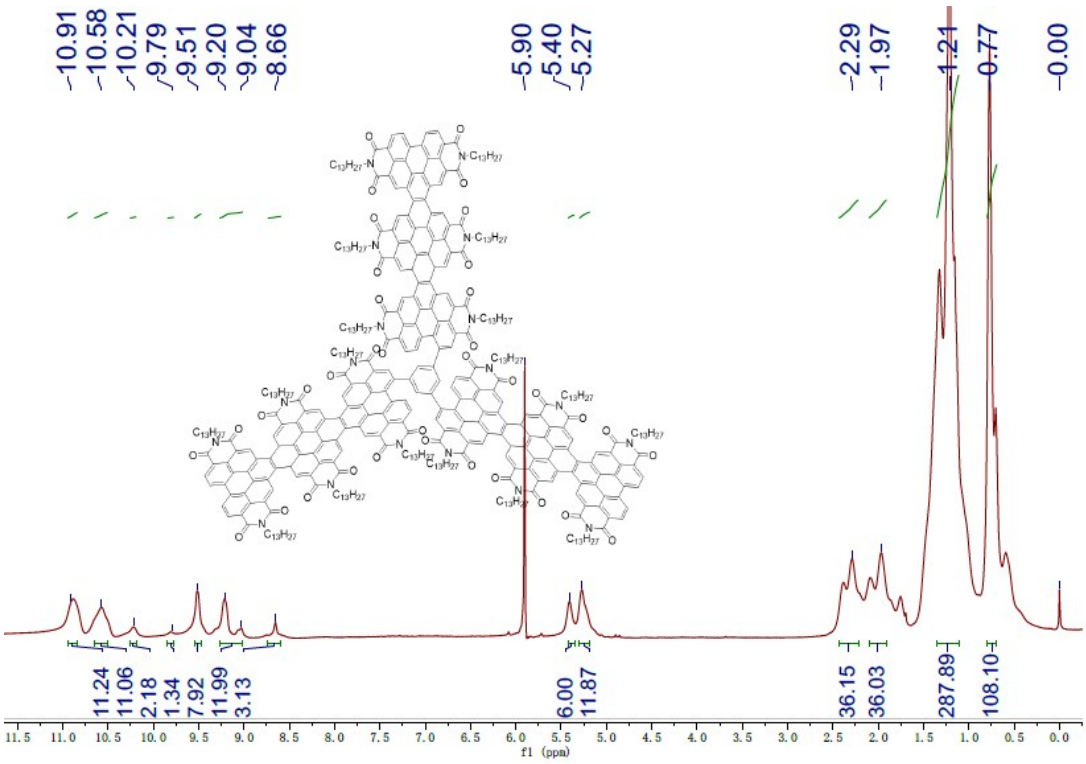

Fig. S12 ^{1}H NMR spectra for TPDI3

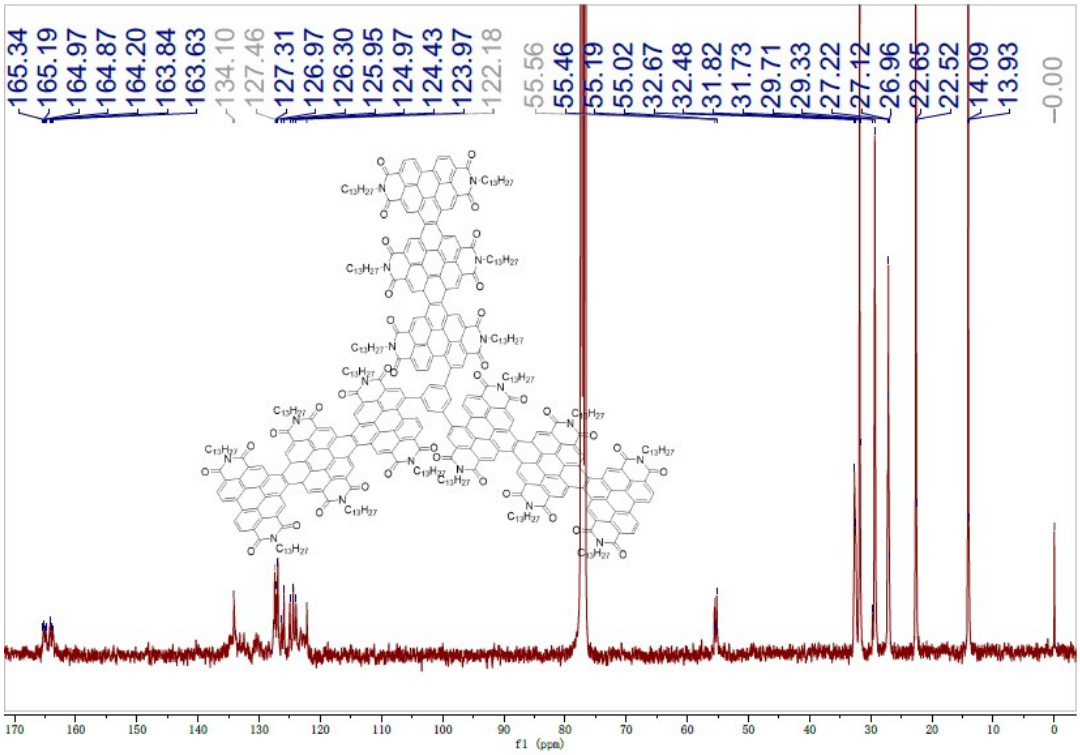

Fig. S13 [13] C NMR spectra for TPDI3

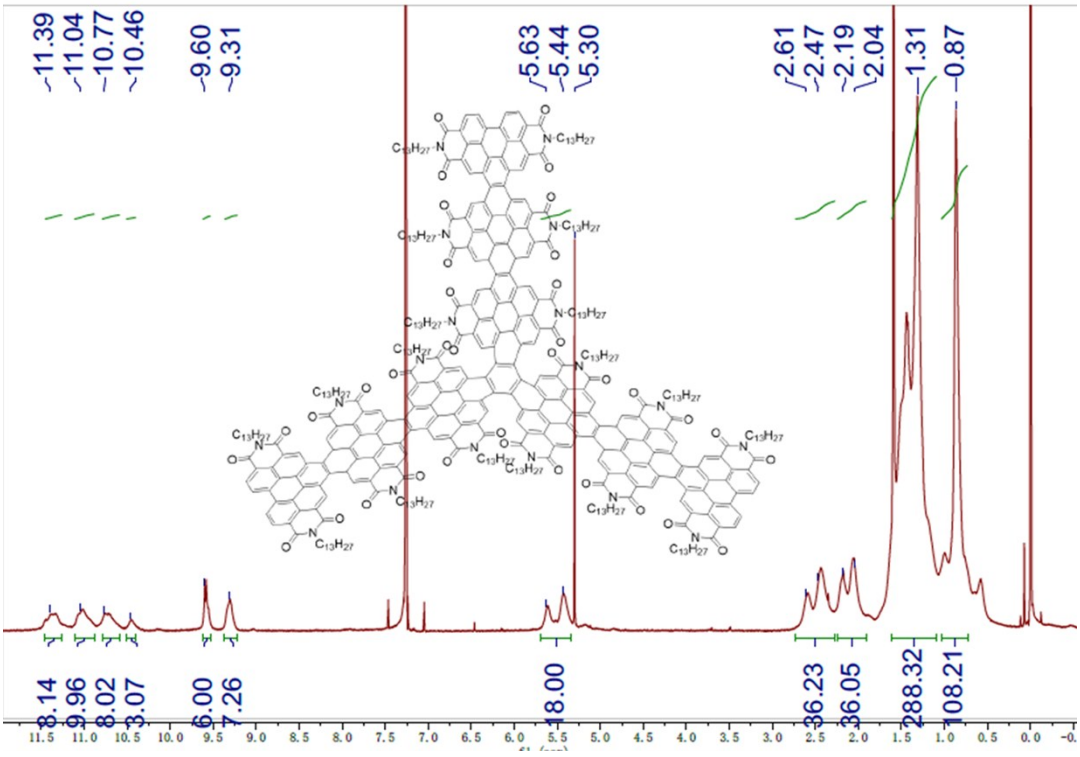

Fig. S14 [1]H NMR spectra for FTPDI3

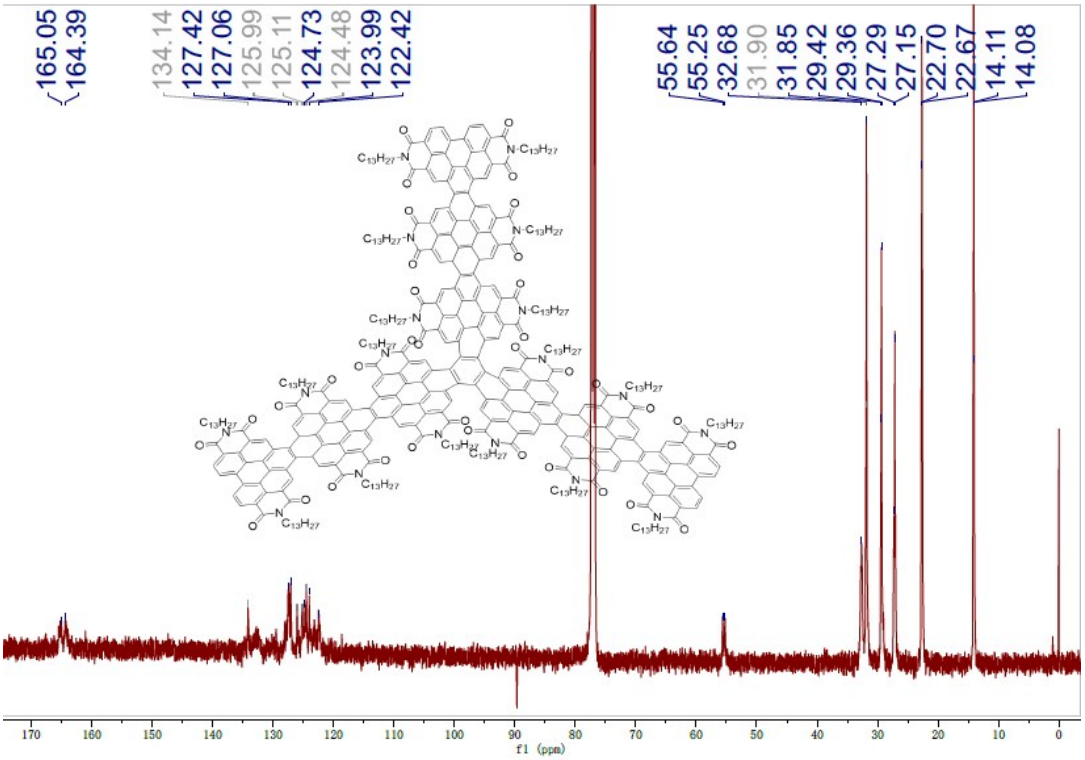

Fig. S15 ^{13}C NMR spectra for FTPDI3

12. MALDI-TOF Mass Spectrum

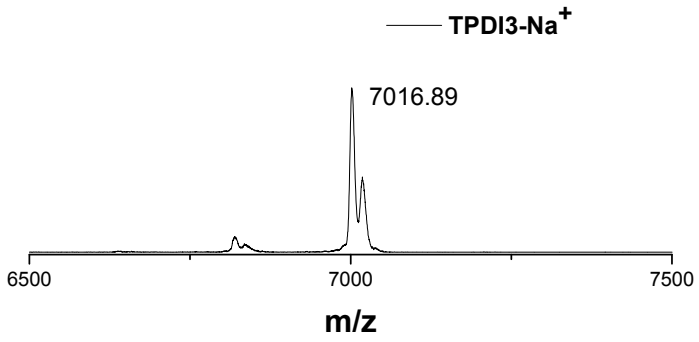

Fig. S16 MALDI-TOF Mass Spectrum for TPDI3

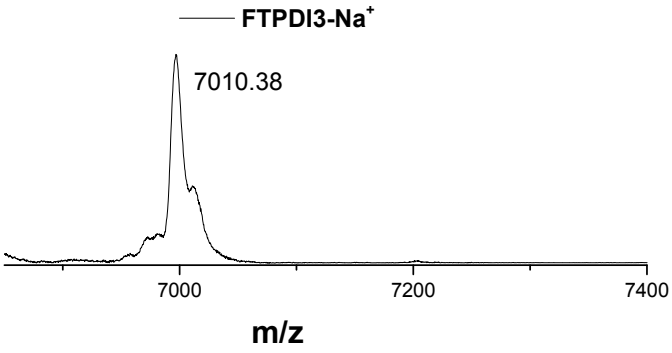

Fig. S17 MALDI-TOF Mass Spectrum for FTPDI3

References:

1. T. J. Sisto, Y. Zhong, B. Zhang, M. T. Trinh, K. Miyata, X. Zhong, X. Y. Zhu, M. L. Steigerwald, F. Ng, C. Nuckolls, *J. Am. Chem. Soc.*, 2017, **139**, 5648-5651.
2. A. Wicklein, A.Lang,, M. Muth, M. Thelakkat, *J. Am. Chem. Soc.*, 2009, **131**, 14442-14453.
3. P. Rajasingh, R. Cohen, E. Shirman, L. J. W. Shimon, B. Rybtchinski, *J. Org. Chem.*, 2007, **72**, 5973-5979.
4. Y. Zhong, M. T. Trinh, R. Chen, W. Wang, P. P. Khlyabich, B. Kumar, Q. Xu, C. Y. Nam, M. Y. Sfeir, C. Black, M. L. Steigerwald, Y. L. Loo, S. Xiao, F. Ng, X. Y. Zhu, C. Nuckolls,. *J. Am. Chem. Soc.*, 2014, **136**, 15215-15221.
5. J. P. Perdew, K.Burke, M. Ernzerhof, *Phys. Rev. Lett.*, 1996, **77**, 3865-3868.
6. J. P. Perdew, K. Burke, M. Ernzerhof, [Phys. Rev. Lett. 77, 3865 (1996)]. *Phys. Rev. Lett.*, 1997, **78**, 1396-1396.
7. M. J. Frisch, G. W. Trucks, H. B. Schlegel, G. E. Scuseria, M. A. Robb, J. R. Cheeseman, G. Scalmani, V. Barone, G. A. Petersson, H. Nakatsuji, X. Li, M. Caricato, A. V. Marenich, J. Bloino, B. G.Janesko,

R. Gomperts, B. Mennucci, H. P. Hratchian, J. V. Ortiz, A. F. Izmaylov, J. L. Sonnenberg, Williams, F. Ding, F. Lipparini, F. Egidi, J. Goings, B. Peng, A. Petrone, T. Henderson, D. Ranasinghe, V. G. Zakrzewski, J. Gao, N. Rega, G. Zheng, W. Liang, M. Hada, M. Ehara, K. Toyota, R. Fukuda, J. Hasegawa, M. Ishida, T. Nakajima, Y. Honda, O. Kitao, H. Nakai, T. Vreven, K. Throssell, Jr., J. A. Montgomery, J. E. Peralta, F. Ogliaro, M. J. Bearpark, J. J. Heyd, E. N. Brothers, K. N. Kudin, V. N. Staroverov, T. A. Keith, R. Kobayashi, J. Normand, K. Raghavachari, A. P. Rendell, J. C. Burant, S. S. Iyengar, J. Tomasi, M. Cossi, J. M. Millam, M. Klene, C. Adamo, R. Cammi, J. W. Ochterski, R. L. Martin, K. Morokuma, O. Farkas, J. B. Foresman, D. J. Fox, Gaussian 16 Rev. B.01, Wallingford, CT, 2016.

8. T. Lu, F. Chen, *J. Comput. Chem.*, 2012, **33**, 580-592.
9. W. Humphrey, A. Dalke, K. Schulten, *J. Mol. Graphics*, 1996, **14**, 33-38.
10. Y. Zhong; M. T. Trinh; R. Chen; W. Wang; P. P. Khlyabich; B. Kumar; Q. Xu; C. Y. Nam; M. Y. Sfeir; C. Black; M. L. Steigerwald; Y. L. Loo; S. Xiao; F. Ng; X. Y. Zhu; C. Nuckolls, *J. Am. Chem. Soc.*, 2014, **136**, 15215-15221.
11. Y. Zhong; M. T. Trinh; R. Chen; G. E. Purdum; P. P. Khlyabich; M. Sezen; S. Oh; H. Zhu; B. Fowler; B. Zhang; W. Wang; C. Y. Nam; M. Y. Sfeir; C. T. Black; M. L. Steigerwald; Y. L. Loo; F. Ng; X. Y. Zhu; C. Nuckolls, *Nat. Commun.*, 2015, **6**, 8242.
12. T. J. Sisto; Y. Zhong; B. Zhang; M. T. Trinh; K. Miyata; X. Zhong; X. Y. Zhu; M. L. Steigerwald; F. Ng; C. Nuckolls, *J. Am. Chem. Soc.*, 2017, **139**, 5648-5651.
13. G. Gao; N. Liang; H. Geng; W. Jiang; H. Fu; J. Feng; J. Hou; X. Feng; Z. Wang, *J. Am. Chem. Soc.*, 2017, **139**, 15914-15920.
14. M. Liu; J. Yang; C. Lang; Y. Zhang; E. Zhou; Z. Liu; F. Guo; L. Zhao, *Macromolecules*, 2017, **50**, 7559-7566.
15. Y. Yin; J. Yang; F. Guo; E. Zhou; L. Zhao; Y. Zhang, *ACS Appl. Mater. Interfaces.*, 2018, **10**, 15962-15970.
16. M. Liu; J. Yang; Y. Yin; Y. Zhang; E. Zhou; F. Guo; L. Zhao, *J. Mater. Chem. A*, 2018, **6**, 414-422.
17. Y. Guo; Y. Li; O. Awartani; H. Han; J. Zhao; H. Ade; H. Yan; D. Zhao, *Adv. Mater.*, 2017, **29**, 1700309.
18. T. A. Shastry; P. E. Hartnett; M. R. Wasielewski; T. J. Marks; M. C. Hersam, *ACS Energy Lett.*, 2016, **1**, 548-555.
19. Y. Yin; J. Song; F. Guo; Y. Sun; L. Zhao; Y. Zhang, *ACS Appl. Energy Mater.*, 2018, **1**, 6577-6585.
20. M. Wu; J. P. Yi; L. Chen; G. He; F. Chen; M. Y. Sfeir; J. Xia, *ACS Appl. Mater. Interfaces.*, 2018, **10**,

27894-27901.